The Total Number of Acini Remains Constant throughout Postnatal Rat Lung Development

Sébastien F. Barré[1], David Haberthür[2], Tiziana P. Cremona[1],

Marco Stampanoni[2, 3], and Johannes C. Schittny[1].

[1] Institute of Anatomy Bern, University of Bern, Bern, Switzerland

[2] Swiss Light Source, Paul Scherrer Institute, Villigen, Switzerland

[3] Institute for Biomedical Engineering, Swiss Federal Institute of Technology and University of Zürich, Zürich, Switzerland.

Correspondence.   Johannes C. Schittny

University of Bern, Institute of Anatomy,

Baltzerstrasse 2, CH-3012 Bern, Switzerland

Phone +41 31 631 4635, FAX +41 31 631 3807,

E-mail: johannes.schittny@ana.unibe.ch

Abstract

The pulmonary airways are subdivided into conducting and gas-exchanging airways. The small tree of gas-exchanging airways which is fed by the most distal conducting airway represents an acinus. Very little is known about the development of the number of acini. The goal of this study was to estimate their number throughout rat postnatal development. Right middle rat lung lobes were obtained at postnatal day 4-60, stained with heavy metals, paraffin embedded, and scanned by synchrotron radiation based X-ray tomographic microscopy or imaged using micro computed tomography after critical point drying. The acini were counted by detection of the transitional bronchioles (bronchioalveolar duct junction; BADJ) using morphological criteria (thickness of the walls of airways and appearance of alveoli) during examination of the resulting 3D image stacks. Between postnatal days 4-60, the number of acini per lung remained constant (5840 ± 547 acini), but their volume increased significantly. We conclude that the acini are formed before the end of the saccular stage (before postnatal day 4) and that the developmental increase of the lung volume is achieved by an increase of the acinar volume and not by an increase of their number. Furthermore, our results propose that the bronchioalveolar stem cells, which are residing in the BADJ, are as constant in their location at the BADJ itself.

Introduction

50

In 1974, P. H. Burri explained (8): "Another type of alveolar formation consists in the transformation of originally purely conducting into respiratory airways" and in 1984 (7): "The branching pattern and structure of conducting airways are mature at birth, so that except for the terminal bronchiole (where transformation into respiratory passage may occur) the adult bronchial tree is the replica of the newborn one". His statements were based on observations made by Boyden and Tompsett on bronchial trees of human infants and dog puppies (5, 6). To our best knowledge — due to the complexity of lung architecture and to technical limitations — nobody has quantitatively followed the development of the pulmonary acini until now.

60

The term acinus (plural: *acini*) is generally used to describe the few generations of the bronchial tree which are located distally of a terminal bronchiole. The latter is defined as the most distal purely conducting generation of airways. One acinus represents the functional unit of the lung. Because rat belong to the animals which do not possess respiratory bronchioles (41) a transitional bronchiole opens directly into the most proximal alveolar duct(s) of the acinus. The transitional bronchioles contain the bronchioalveolar duct junction where the bronchioalveolar stem cells are located. In human lungs, which possess respiratory bronchioles (41) the entrance of the acini is defined at the junction of the terminal and respiratory bronchioles. The bronchioalveolar junction is defined as the entrance of a ventilator unit (38). Again at this junction the bronchioalveolar stem cells are located. Therefore, the best human correlate of the rat acinus is the human ventilator unit.

74   Due to their complex three-dimensional structure, acini cannot be detected by two-dimensional investigations. Therefore, several approaches were proposed to

76   overcome this limitation. Casting methods were used by Yeh et al. (46) and by Rodriguez et al. (24). Serial-sectioning was used by Mercer and Crapo (21), while

78   Wulfsohn et al. (45) developed an estimation technique based on a disector of five consecutive sections. However, as explained in Barré et al. (3) these methods

80   require tedious work, and thus are not suited for studies with larger number of samples. Several publications proposed approaches based on X-ray tomography

82   (10, 17, 18, 20, 34-36, 42). Even if the latter approach would be suitable for the analysis of larger number of sample, to our best knowledge, it has not been done

84   until now, especially not for the analysis of the development of the acini.

86   Lung developmental is divided in the embryonic, fetal, and postnatal periods (7, 30, 33, 44). In the embryonic period, the lung anlage appears as two independent

88   outpouchings of the foregut forming the two lung buds. The formation of the airways starts shortly afterwards by branching morphogenesis which is defined as a repetitive

90   branching and outgrowth of the future airways. Typically, in human lungs, the branching of the airways follows a dichotomous pattern. This means that the airways

92   symmetrically branch into two smaller airways of the same diameter. With the appearance of the pleura the embryonic period blends over into the fetal period.

94   Branching morphogenesis continues and at the end of the pseudoglandular stage approximately 20 airway generations are formed in humans (16). The airway

96   formation continues during the next step, the canalicular stage. At the end of this stage the transition between conducting and gas-exchanging airways is detectable,

98   resulting in the "birth of the acinus" (4) even if the proximal part of the acinar airways is already formed during the pseudoglandular stage. Branching morphogenesis

100   comes to its end at latest during the saccular stage, by the arising of saccules and of

the type 1 and 2 alveolar epithelial cells at the distal ends of the bronchial tree. The

102   next and final stage, alveolarization, is composed of two phases (classic and

continued) (32, 39) which ends during young adulthood (12, 14, 31). This description

104   of the stages of lung development is in general valid for all mammalians

independently of their airways branching pattern (28). The main differences are found

106   in the duration of the stages and at the time point of birth.

108   While human lungs possess a dichotomous branching pattern, lungs of rats and

other rodents possess a monopodial one (23, 46). At most of the branching points

110   the airway divides asymmetrically into one larger and one smaller airway. In rats, the

trachea divides into two main bronchi from which main lobar bronchi, one per lobe,

112   emerge to ventilate the five lung lobes. A system of secondary and tertiary lobar

bronchi arises from the next larger category to ventilate the peripheral parts of the

114   lobes. Acini are directly connected by transitional bronchioles to purely conducting

airways of various generations, even including secondary lobar bronchi (3, 24).

116

The goal of this study was to estimate the number of acini for rats at different ages

118   (postnatal days 4, 10, 21, 36, and 60). Taking P.H. Burri's statements (7, 8) as

starting point, we studied the development of the pulmonary acini in rats. We used a

120   time-efficient estimation protocol developed in our laboratory (3) in order to

investigate large amounts of samples. Surprisingly, the number of acini showed no

122   statistical differences between the days studied indicating that the number of acini

remains constant during lung development. Furthermore we conclude that the

124   positions of the entrance of the acini, as well as the sites where the bronchioalveolar

stem cells are residing, are defined in the bronchial tree before the end of the

126   saccular stage.

128

Materials and Methods
130

132   **Animals.** Lungs of twenty-seven male rats (postnatal days 4, 10, 21, 36, and 60; Wistar Bern) were obtained after fixation with 4% paraformaldehyde in phosphate

134   buffered saline via tracheal instillation at a constant pressure of 20 cm water column. The lung was removed from the chest cavity and the pressure was maintained during

136   fixation for a minimum of two hours at 4°C in order to prevent a recoiling of the lung (19, 22, 40). After fixation, all lobes were separated and their volume was measured

138   by water displacement (26). A second volume measurement was performed using the Cavalieri principle (9) on the tomographic dataset to determine the shrinkage

140   factor of the samples.

142   All animal studies were approved by and conducted in accordance with the Veterinary Service of the Canton of Bern, Switzerland and the Swiss Federal Agency

144   for Environment, Forest and Landscape.

146   **X-ray Tomography.** Two tomographic methods were used during this study: synchrotron radiation based x-ray tomographic microscopy (SRXTM) and micro

148   computed tomography (µCT). The right middle lung lobes were prepared, as already described (3, 25), either by critical point drying for µCT (15) or by heavy metal

150　staining with osmium tetroxide and uranyl acetate (33), and paraffin embedding for

SRXTM.

152

Synchrotron radiation based x-ray tomographic microscopy. 20 samples were

154　scanned at the TOMCAT beamline (37) of the Swiss Light Source synchrotron facility

at the Paul Scherrer Institute (Villigen, Switzerland). X-rays at energy of 20 keV were

156　converted to visible light by a scintillator (20 µm thick LuAG:Ce or 18 µm thick

YAG:Ce, Crytur Ltd., Turnov, Czech Republic) after passing the samples. An optic

158　microscope magnified the visible light in order to obtain effective voxel size lengths of

1.75 to 3.5 µm. In order to visualize the entire lung lobe, the field of view of the

160　microscope was increased perpendicular to the rotational axis using 'wide-field

SRXTM' (three field of views) (11) or 360° scans (two field of views). In addition, five

162　to seven wide-field scans were stacked parallel to the rotational axis, resulting in 3D-

stacks of 8 bit grayscale images of up to 7500x7500 pixels per slice.

164

Micro computed tomography. Seven samples were imaged by a µCT device

166　(SkyScan 1172, Bruker, Billerica, MA, USA) at 33 kV and 204 µA without filtering.

Two to three oversize scans in the vertical direction were needed to visualize the

168　entire sample at 2.5-3.5 µm voxel side length. The GPU reconstruction software

(NReconServer64bit, Bruker, Billerica, MA, USA) was used on a GeForce GTX 680

170　graphic card (Nvidia Corp., Santa Clara, Ca, USA) to create 8 bit grayscale image

stacks of approximately 4000x4000x2500 voxels per scan. Additional samples (right

172　upper, right lower, cardiac lobe and left lung) at days 4 and 60 were also scanned in

the µCT.

174

Detection and Counting of Acini. The manual acini counting followed the protocol described by Barré et al. (3). The acini entrances (i.e. transition from conducting to gas-exchanging airways) were detected based on morphological criteria (thickness of airway walls and appearance of alveoli) by scrolling through tomographic data sets representing right middle lung lobes (n = 27). In addition, three entire lungs were counted at days 4 and 60 to validate that the right middle lobe is a valid estimator of the entire lung. The software Fiji (27) was used to crop and display sub-stacks of 250 to 500 images, in order to reduce the computing power requirement, and to manually label the detected acini entrances. The labels were manually counted using a laboratory counter (Clay Adams, New York, USA). After one sub-stack was counted, labels of overlapping acini were reported to the next sub-stack to exclude double counting. All data were analyzed on a Dell Precision T5500 work station (Intel Xeon X5650 (six Core, 2.67 GHz), 24 GB RAM, Windows 7 Professional 64).

Three-dimensional Visualization. The conducting airways of five right middle lung lobes (one per developmental time point) were visualized three-dimensionally adapting a protocol described by Barré et al. and Haberthür et al. (3, 10). Briefly, several images stacks of 250-500 eight bit greyscale images were analyzed using MeVisLab (version 2.1, 2010-07-26 Release, MeVis Medical Solutions and Frauenhofer MEVIS-Institute for Medical Image Computing, Bremen, Germany). The sub-stacks were loaded as TIFF files and segmentation stoppers were manually set at the acinar entrances to separate them from the conducting airways. The conducting airways were segmented using a gray-level threshold-based region growing algorithm (47) after down-sampling with a factor of 2. The segmentation seed points were manually set within the conducting airways. All segmentations were reconstructed as one 3D model using a custom-made MeVisLab pipeline. This basic

pipeline stacked all segmentations and displayed spheres at the position of the

202   segmentation stoppers.

204   **Statistics.** The statistical analysis was done using Microsoft Excel (version 14.0.7106.5003, 32-bit) and Prism (version 5.04, GraphPad Software Inc.). The

206   values are expressed as means (± standard deviation). The linear regression of the observed values and the R^2 (coefficient of determination) were calculated. This

208   coefficient indicates how well the observed values fit the ideal values of a linear regression. In this case, R^2 is the square of the Pearson correlation coefficient (r). No

210   correlation between parameters was assumed when $R^2 \leq 0.5$ ($|r| \leq 0.7$), weak correlation when $0.5 < R^2 \leq 0.7$ ($0.7 < |r| \leq 0.84$), and strong correlation when $0.7 <$

212   R^2 ($0.84 < |r|$). In addition, multiple regression and ANOVA F-tests were used (both using the data analysis toolbox on Microsoft Excel)(1). A multiple regression test was

214   used to determine if observations groups were correlating. To do so, one group was expressed as the dependent variable and the others as independent variables. The

216   predicted values (i.e. regression results) were compared to the values of the group set as dependent variable using the coefficient of determination. The standard score

218   (difference of observation and group mean divided by group standard deviation) was used to normalize the data prior to regression analysis. The significance of difference

220   between the means of observation groups was achieved using a T-test or using one way ANOVA F-test. A significance level of $\alpha = 95\%$ was used for both tests, detecting

222   significant difference if $p \leq 0.05$ or non-significant difference if $p > 0.05$. In addition to ANOVA, a Bonferroni's multiple comparison tests was performed to define which

224   group was significantly different from the other groups (1). T-test and ANOVA require normal distributed data. Therefore QQ-plots were used to test for normal-distributed

226   values.

228   **Calculations**. The total number of acini present in a rat lung was calculated by dividing the counted number of acini in the right middle lobe by the parenchymal

230   volume of the corresponding lobe and by multiplying this result with the total parenchymal volume. The mean acinar volume (tissue plus airspace of an acinus)

232   was calculated by dividing the lobe volume by the counted number of acini and multiplied by the volume density of parenchyma (Tab. 1). The parenchymal volume

234   density was estimated according to the ATS guidelines (13).

236

238   **Results**

240   **Detection of the acinar entrance throughout lung development**. In tomographic datasets morphological criteria (thickness of the airways walls and appearance of

242   alveoli) were used to detect the entrances of the acini (Fig. 1) as described in Barre et al. (2). Because the acini are not fully developed and the alveoli not yet formed at

244   day 4, we used the appearance of the gas-exchanging capillaries in the walls of the airspaces as additional, newly introduced criterion for the detection of the acinus

246   entrance. Due to the iron contained within the erythrocytes, the contrast inside the capillaries was large enough to be safely detected. This criterion was also used at

248   day 10, while it was not necessary to be used for lungs at older age. Although acinar airways are still immature, the alveolar duct already presents its typical shape (airway

250   walls covered with uprising new alveolar septa) at the beginning of the stage of alveolarization. The latter contrasted with the tubular wall of the conducting airways.

252   Therefore, we used it as the second additional criterion for the detection of the transition between conducting and gas-exchanging airways.

254

Growth of lobe volume. We compared the growth of the five lung lobes throughout

256   postnatal lung development (Tab. 2). In particular, we asked if its fraction of the total lung volume changes during development. No significant changes were observed for

258   the right upper, right middle, and right lower lobe (Tab. 2). However, the fraction of the left lung decreased between postnatal days 4-10 and subsequently stays

260   constant. The volume fraction of the cardiac lobe increases inversely proportional to the left lung between postnatal days 4-10. Afterward only a small additional increase

262   was observed until day 60.

264   **Validation of the sampling.** According to Barré et al. (3), the right middle lung lobe is a valid estimator of the number of acini for the entire lung for adult rats. The

266   estimation was based on the parenchymal volume of the entire lung and of the right middle lobe. In order to test if the right middle lobe is also a valid estimator for

268   immature lungs, all acini of three entire lungs at postnatal day 4 were counted manually. This counting showed that the mean acinar volume of the right middle lobe

270   (0.066 μl) was not statistically different from the mean acinar volume of right upper (0.065 μl) and right lower lobes, as well as of the entire lung (0.073 μl) and of the

272   sum of the left lung and the cardiac lobe (0.081 μl / Tab. 3). We chose this sum, because during postnatal development the volume of the cardiac lobe growth

274   unproportional to the three other right lung lobe (see above). However, the sum of the volume of the left lung and the cardiac lobe growth proportional to the three other

276   lobes (Tab. 2). Based on the mean acinar volume the mean number of acini (6469 ± 720 acini) was estimated for these three samples following the method presented

278   previously (3). No statistical difference was observed between the counted (5865 ±

465 acini) and the estimated (6469 ± 720 acini) number of acini at postnatal day 4.

280   The counted number of acini per lobe (N=3 for right upper, right middle, right lower,

cardiac, and left lung) between days 4 and 60 (3) showed no statistical differences. In

282   addition, the mean of the observed difference between estimated and counted total

number of acini was approximately 10%. Collectively, these findings support the view

284   that the right middle lung lobe is a valid estimator for the total number of acini at any

stage of postnatal lung development.

286

Number of Acini. The number of acini in the right middle lung lobes were counted at

288   postnatal days 4, 10, 21, and 36 as previously described and compared to data of the

adult lung (day 60) (3). No significant differences were observed between the five

290   age groups (Tab. 4). Therefore, in opposite to body weight and lung volume, the

number of acini is constant throughout postnatal lung development. We detected no

292   direct correlation between these three lung parameters. However, the variation to the

mean can be calculated for all individuals over the five time points. To do so, in a

294   multiple regression analysis the standard scores (difference of mean and individual

value divided by the standard deviation) of body weight and lung volume of all 27

296   animals were set as the independent variables, and the number of acini of the right

middle lobe was set as the dependent variable. The analysis provided a value (Fig. 2,

298   predicted curve) for every sample. Assuming a linear relationship between all three

tested parameters, the predicted values should match with the observed number of

300   acini (Fig. 2). This was not the case (R^2 = 0.08), and thus the number of acini, body

weight, and lung volume showed **no** linear correlations.

302

Mean acinar volumes. The mean acinar volume (Tab. 5), defined as the parenchymal lobe volume divided by the counted number of acini, was calculated for the right middle lobe at day 4, 10, 21, 36, and 60. Based on the specific acinar volume (Tab. 5) a bi-phasic growth of the acinar volume was observed (Fig. 3). Hence, the acinar volume increases proportionally to body weight until day 21, while after day 21 body weight grows faster than acinar volume. This kind of bi-phasic growth was already reported for the lung volume, the anlage of new alveolar septa, and for the number of alveoli by Burri (8), Schittny (32), and Tschanz (40), respectively.

Shrinkage of samples. Large shrinkage factors have been reported for paraffin embedding (28.70 ± 0.62 %) and for critical point drying (62.0 ± 1.5 %) both measured at day 60 (3). In the present study, we analyzed the shrinkage factor of the right middle lobe for all five remaining time points. The volume of paraffin embedded samples showed a reduction of 24.6 % (± 4.4) and the ones of the critical point dried samples decreased by 62 % (± 1.5).

Reconstruction of conducting airways. In order to visualize our results, we reconstructed the conducting airways of one right middle lobe per time point (Fig. 4). The visualization highlighted the high similarity of the conducting airways pathway at any time point and between the individuals. Most of the conducting airways ended with one acinar entrance being located on a transitional bronchiole. However, we also detected acinar entrances very close to each other. In this case, a branching point was located inside the transitional bronchiole (Fig. 4) as already reported in Barré (3).

Discussion

332   Previous studies by Burri et al. (7, 8) and Boyden & Tompsett (5, 6) proposed that originally purely conducting bronchioles may be transformed into respiratory airways

334   during early alveolarization. To our best knowledge the presented study represents the first quantitative investigation of the development of the number of acini

336   throughout lung development in rats. We were able to show that the number of acini stays constant from day 4 to young adulthood (Tab. 4). From the structural point of

338   view we did not observe any shift of the acinus entrance or the bronchoalveolar duct junction within the bronchial tree. Initially, we expected a proximal shift of the acinus

340   entrances and a dramatic, approximately factor of 2 decrease of the number of acini. Our investigations throughout postnatal lung development did not show any statistical

342   difference of the number of acini. At an early stage of alveolarization (day 4 postnatal) 6326 ± 497 acini were estimated for the entire lung. A similar number

344   (5612 ± 547) was observed in young adult rats at postnatal day 60. We conclude that the acini are formed before the end of the saccular stage (before postnatal day 4)

346   and that the developmental increase of the lung volume is achieved by an increase of the acinar volume and not by an increase of the number of acini. According to

348   Kitaoka et al. (16) the formation of the airways is completed up to the acinar airways at the end of the pseudoglandular stage. During the canalicular stage, epithelial

350   differentiation takes place and the bronchioalveolar duct junction, the border between the conducting airways and the gas-exchange region, is formed (29). Because no

352   shift of the acinus entrance occurs and no additional conducting airways are created, we conclude that the number of acini will not change during alveolarization.

354   The bronchioalveolar duct junction contains the so called bronchioalveolar stem cells which are very important for homeostasis and repair. Because the location of the

356   acinar entrance or better the bronchioalveolar duct junction does not move during alveolarization, the site where these stem cells are residing, stays also constant.

358

        Our conclusions, based on rat lungs, are at a first view in contradiction with the

360   observations of Boyden and Tompsett (5, 6). They observed a reduction of the non-respiratory generation between newborn and adult in humans and dogs. The

362   difference may be explained by the different architecture of rat, dog, and human airways. Rats possess one generation of transitional bronchioles instead of few

364   generations of respiratory bronchioles (24) which are found in dogs and humans. Thus, for rats, the acinus entrance is located at the bronchioalveolar duct junction

366   where the epithelium of the bronchioles (club cells and ciliated cells) blends over into the alveolar epithelium. The correlating structural in humans is the ventilatory unit

368   and not the acinus (see introduction). Therefore, Boyden and Tompsett (5, 6) described the alveolarization of the respiratory bronchioles and not a movement of

370   the bronchioalveolar duct junction. If the correlating structure of humans and rat are correctly compared, no contradiction between the presented data and Boyden and

372   Tompsett observations (5, 6) are present.

374   Our detection method did not only focus on the appearance of alveoli for the detection of the acini entrances, but also on the airway wall thickness, on the

376   appearance of alveolar capillaries, and on the shape of the airways. Because of that, we were able to detect the transition between the conducting and the gas-

378   exchanging parts of the transitional bronchiole even before alveoli were present. As a consequence, the number of acini could be counted prior to the beginning of the

380   alveolarization. We conclude that, for rat lungs, the final number of acini is reached at the latest by the end of the saccular stage.

382

The localization of the acini entrances represents an important additional observation

384   (Fig. 4, colored spheres). They are inhomogenously distributed over the entire lobe, in close proximity to the larger airways. As a result a cortical region exists near the

386   pleura which is free of any acinus entrances. Due to the monopodial branching pattern (46) the most proximal acinus is located at intra-lobar generation four,

388   whereas distal acini are located at much higher generations (Fig. 4). Lee et al. (17, 18) used X-ray tomography of silicon casts of the airways to analyze and count the

390   generations and segments of the conducting airways. We propose that an estimation of the number of acini, based on their method may be biased due to the

392   inhomogeneous distribution of the entrances of the acini in species possessing a monopodial branching pattern. To eliminate any dependency of the results on the

394   kind of branching pattern, we counted all acinar entrances in one lobe.

396   We compared the bronchial tree down to the acinar entrances between days 4 and 60 (Fig. 4). The shown bronchial trees were obtained of five different individuals.

398   Therefore, we are comparing different developmental stages and individual animals at the same moment. We observed a high similarity and no change in complexity

400   between the five analyzed bronchial trees. We conclude that once the bronchial tree is formed it stays very constant during lung development and that a proportional

402   growth takes place during postnatal rat lung development. In addition, the individual alterations appear to be small and at a similar level as variations observed in the

404   branching of larger blood vessels. The number and the localization of the secondary and tertiary lobar airways (43) demonstrated this similarity.

406 Previously, we demonstrated that the right middle lung lobe is a valid estimator for

408 the number of acini for the entire lung (3). However, our method assumes a direct

correspondence between the number of acini per lobe and the fraction of total lung

410 volume of this particular lobe. A variation of the fraction of total lung volume was

observed for the left lung and the cardiac lobe between days 4 and 10 (Tab. 2). To

412 investigate if these variations influenced the estimation method, the number of acini

of three entire lungs were manually counted at day 4 (5865 ± 465 acini) and

414 compared with the results obtained at day 60 (5943 ± 521 acini) (3). No statistical

differences were observed between the counted numbers of acini at these two time

416 points. This demonstrated that at day 4 the acinar development of cardiac lobe is at a

similar state as the other four lobes. The observed variations of the fraction of total

418 lung volume had no influence on the estimation of the total number of acini based on

the right middle lobe. However, due to these variations the number of acini cannot be

420 estimated for the single lobes at postnatal day 4, as proposed in Barré et al. (3). To

overcome this problem cardiac lobe and left lung have to be considered as one entity

422 (Tab. 3) for the calculations. When the cardiac lobe and the left lung are combined as

one entity, the mean acinar volume of the right middle lobe does not statistically differ

424 with the mean acinar volume of any other lobe (p = 0.198, Tab. 3). Thus, we

conclude that the right middle lobe is also a valid estimator for the entire lung

426 development.

428 In summary, we conclude that the total number of acini is constant throughout lung

development but can differ between individuals. No relationships were detected with

430 other parameters like total lung volume, surface area, etc. Combining our method

with others (10, 17) it will be possible to further characterize conducting airways and

432 gas-exchanging regions. This will hopefully lead to a better understanding of clinical relevant topics, for instance air-flow within the lung, pulmonary particle depositions, 434 or lung regeneration.

436

Acknowledgement

444 **Disclosures**. No conflict of interest, financial or otherwise

446 **Author Contributions.** S.F. Barré, obtained and scanned samples, developed the procedure and performed the counting of the acini, analyzed data and drafted the 448 manuscript. D. Haberthür obtained and scanned samples, contributed to the development of the procedure of the counting of the acini and to the writing of the 450 manuscript. T.P. Cremona contributed to writing. M. Stampanoni designed and built the beamline. J.C. Schittny conceived and designed the study, obtained and scanned 452 samples, analyzed data and contributed to writing.

454

References

456

1.   **Altman DG**. *Practical statistics for medical research*. London: Chapman & Hall/CRC,

458   1991.

2.   **Barre SF, Haberthür D, Stampanoni M, and Schittny JC**. Efficient estimation of the

460   total number of acini in adult rat lung. *Physiol Rep* 2: 46-53, 2014.

3.   **Barré SF, Haberthür D, Stampanoni M, and Schittny JC**. Efficient estimation of the

462   total number of acini in adult rat lung. *Physiological reports* 2: e12063, 2014.

4.   **Boyden E**. Development of the lung. *Lung biology in health and disease Dekker, New*

464   *York* 3-35, 1977.

5.   **Boyden E, and Tompsett D**. The changing patterns in the developing lungs of infants.

466   *Cells Tissues Organs* 61: 164-192, 1965.

6.   **Boyden E, and Tompsett D**. The postnatal growth of the lung in the dog. *Cells Tissues*

468   *Organs* 47: 185-215, 1961.

7.   **Burri PH**. Fetal and postnatal development of the lung. *Annual review of physiology* 46:

470   617-628, 1984.

8.   **Burri PH**. The postnatal growth of the rat lung III. Morphology. *The Anatomical Record*

472   180: 77-98, 1974.

9.   **Gundersen H, and Jensen E**. The efficiency of systematic sampling in stereology and

474   its prediction*. *Journal of Microscopy* 147: 229-263, 1987.

10.   **Haberthür D, Barré SF, Tschanz SA, Yao E, Stampanoni M, and Schittny JC**.

476   Visualization and stereological characterization of individual rat lung acini by high-resolution

X-ray tomographic microscopy. *Journal of Applied Physiology* 115: 1379-1387, 2013.

478   11. **Haberthür D, Hintermüller C, Marone F, Schittny JC, and Stampanoni M**. Radiation

dose optimized lateral expansion of the field of view in synchrotron radiation X-ray

480   tomographic microscopy. *Journal of Synchrotron Radiation* 17: 590-599, 2010.

12. **Herring MJ, Putney LF, Wyatt G, Finkbeiner WE, and Hyde DM**. Growth of alveoli

482   during postnatal development in humans based on stereological estimation. *American journal*

of physiology Lung cellular and molecular physiology 307: L338-344, 2014.

484   13. **Hsia CC, Hyde DM, Ochs M, and Weibel ER**. An official research policy statement of

the American Thoracic Society/European Respiratory Society: standards for quantitative

486   assessment of lung structure. *American journal of respiratory and critical care medicine* 181:

394-418, 2010.

488   14. **Hyde DM, Blozis SA, Avdalovic MV, Putney LF, Dettorre R, Quesenberry NJ, Singh**

P, and Tyler NK. Alveoli increase in number but not size from birth to adulthood in rhesus

490   monkeys. *AmJPhysiol Lung Cell MolPhysiol* 293: L570-L579, 2007.

15. **Kaeslin M, Wehrle I, Grossniklaus-Bürgin C, Wyler T, Guggisberg U, Schittny JC,**

492   **and Lanzrein B**. Stage-dependent strategies of host invasion in the egg–larval parasitoid< i>

Chelonus inanitus</i>. *Journal of insect physiology* 51: 287-296, 2005.

494   16. **Kitaoka H, Burri PH, and Weibel ER**. Development of the human fetal airway tree:

analysis of the numerical density of airway endtips. *The Anatomical Record* 244: 207-213,

496   1996.

17. **Lee D, Fanucchi MV, Plopper CG, Fung J, and Wexler AS**. Pulmonary architecture in

498   the conducting regions of six rats. *The Anatomical Record* 291: 916-926, 2008.

18. **Lee D, Srirama PK, Wallis C, and Wexler AS**. Postnatal growth of tracheobronchial

500   airways of Sprague–Dawley rats. *Journal of anatomy* 218: 717-725, 2011.

19. **Luyet C, Burri PH, and Schittny JC**. Pre-and postnatal lung development, maturation,

502   and plasticity. Suppression of cell proliferation and programmed cell death by

dexamethasone during postnatal lung development. *Am J Physiol Lung Cell Mol Physiol* 282:

504   L477-L483, 2002.

20. **McDonough JE, Yuan R, Suzuki M, Seyednejad N, Elliott WM, Sanchez PG, Wright AC, Gefter WB, Litzky L, and Coxson HO**. Small-airway obstruction and emphysema in chronic obstructive pulmonary disease. *New England Journal of Medicine* 365: 1567-1575, 2011.

21. **Mercer RR, and Crapo J**. Three-dimensional reconstruction of the rat acinus. *Journal of Applied Physiology* 63: 785-794, 1987.

22. **Mund SI, Stampanoni M, and Schittny JC**. Developmental alveolarization of the mouse lung. *Developmental Dynamics* 237: 2108-2116, 2008.

23. **Phalen R, Yeh H, Schum G, and Raabe O**. Application of an idealized model to morphometry of the mammalian tracheobronchial tree. *The Anatomical Record* 190: 167-176, 1978.

24. **Rodriguez M, Bur S, Favre A, and Weibel E**. Pulmonary acinus: geometry and morphometry of the peripheral airway system in rat and rabbit. *American journal of anatomy* 180: 143-155, 1987.

25. **Roth-Kleiner M, Berger TM, Gremlich S, Tschanz SA, Mund SI, Post M, Stampanoni M, and Schittny JC**. Neonatal steroids induce a down-regulation of tenascin-C and elastin and cause a deceleration of the first phase and an acceleration of the second phase of lung alveolarization. *Histochem Cell Biol* 141: 75-84, 2014.

26. **Scherle WF**. A simple method for volumetry of organs in quantitative stereology. *Microscopy* 26: 57-60, 1970.

27. **Schindelin J, Arganda-Carreras I, Frise E, Kaynig V, Longair M, Pietzsch T, Preibisch S, Rueden C, Saalfeld S, and Schmid B**. Fiji: an open-source platform for biological-image analysis. *Nature methods* 9: 676-682, 2012.

28. **Schittny JC, and Burri P**. Development and Growth of the Lung. In: *Pulmonary Diseases and Disorders*McGraw-Hill Medical, 2008.

29. **Schittny JC, and Burri PH**. Development and growth of the lung. In: *Fishman's pulmonary diseases and disorders*, edited by Fishman AP, Elias JA, Fishman JA, Grippi MA, Kaiser LR, and Senior RM. New-York: McGraw-Hill, 2008, p. 91-114.

30. **Schittny JC, and Burri PH**. Morphogenesis of the Mammalian Lung: Aspects of Structure and Extracellular Matrix Components. In: *Lung Development and Regeneration*, edited by Inc MD. New York, Basel, Hong Kong: 2004.

31. **Schittny JC, and Mund SI**. A Re-Examination of the Maturation of the Alveolar Septa Revealed That Microvascular Maturation Takes Place in Parallel to Alveolarization. *Am J Respir Crit Care Med* 177: A317 (ATS poster, manuscript in preparation), 2008.

32. **Schittny JC, Mund SI, and Stampanoni M**. Evidence and structural mechanism for late lung alveolarization. *AmJPhysiol Lung Cell MolPhysiol* 294: L246-L254, 2008.

33. **Schittny JC, Mund SI, and Stampanoni M**. Evidence and structural mechanism for late lung alveolarization. *American Journal of Physiology-Lung Cellular and Molecular Physiology* 294: L246-L254, 2008.

34. **Sera T, Fujioka H, Yokota H, Makinouchi A, Himeno R, Schroter RC, and Tanishita K**. Three-dimensional visualization and morphometry of small airways from microfocal X-ray computed tomography. *Journal of biomechanics* 36: 1587-1594, 2003.

35. **Sera T, Uesugi K, and Yagi N**. Morphometric deformations of small airways and alveoli under quasi-static inflation process. *Journal of physiological anthropology and applied human science* 24: 465-468, 2005.

36. **Sera T, Yokota H, Tanaka G, Uesugi K, Yagi N, and Schroter RC**. Murine pulmonary acinar mechanics during quasi-static inflation using synchrotron refraction-enhanced computed tomography. *Journal of Applied Physiology* 115: 219-228, 2013.

37. **Stampanoni M, Groso A, Isenegger A, Mikuljan G, Chen Q, Bertrand A, Henein S, Betemps R, Frommherz U, B\öhler P, and others**. Trends in synchrotron-based tomographic imaging: the SLS experience. 6318: 63180M-63181, 2006.

38. **Storey WF, and Staub NC**. Ventilation of terminal air units. *J Appl Physiol* 17: 391-397, 1962.

39. **Tschanz S, Salm LA, Barre SF, Roth-Kleiner M, Burri PH, and Schittny JC**. Rat Lungs Show a Biphasic Formation of New Alveoli during Postnatal Development. *J ApplPhysiol* 2014.

40. **Tschanz SA, Salm LA, Roth-Kleiner M, Barré SF, Burri PH, and Schittny JC**. Rat lungs show a biphasic formation of new alveoli during postnatal development. *Journal of Applied Physiology* 117: 89-95, 2014.

41. **Tyler WS**. Comparative subgross anatomy of lungs. Pleuras, interlobular septa, and distal airways. *Am Rev Respir Dis* 128: S32-36, 1983.

42. **Vasilescu DM, Gao Z, Saha PK, Yin L, Wang G, Haefeli-Bleuer B, Ochs M, Weibel ER, and Hoffman EA**. Assessment of morphometry of pulmonary acini in mouse lungs by nondestructive imaging using multiscale microcomputed tomography. *Proceedings of the National Academy of Sciences* 109: 17105-17110, 2012.

43. **Wallau BR, Schmitz A, and Perry SF**. Lung morphology in rodents (Mammalia, Rodentia) and its implications for systematics. *Journal of Morphology* 246: 228-248, 2000.

44. **Woods JC, and Schittny JC**. Lung structure at preterm and term birth. In: *Fetal Lung Development - Clinical Correlates & Future Technologies*, edited by Jobe AH, Whitsett JA, and Abman SH. New York: Cambridge University Press, 2016, p. 126-140.

45. **Wulfsohn D, Knust J, Ochs M, Nyengaard JR, and Gundersen HJG**. Stereological estimation of the total number of ventilatory units in mice lungs. *Journal of Microscopy* 238: 75-89, 2010.

46. **Yeh H, Schum G, and Duggan M**. Anatomic models of the tracheobronchial and pulmonary regions of the rat. *The Anatomical Record* 195: 483-492, 1979.

47. **Zucker SW**. Region growing: Childhood and adolescence. *Computer graphics and image processing* 5: 382-399, 1976.
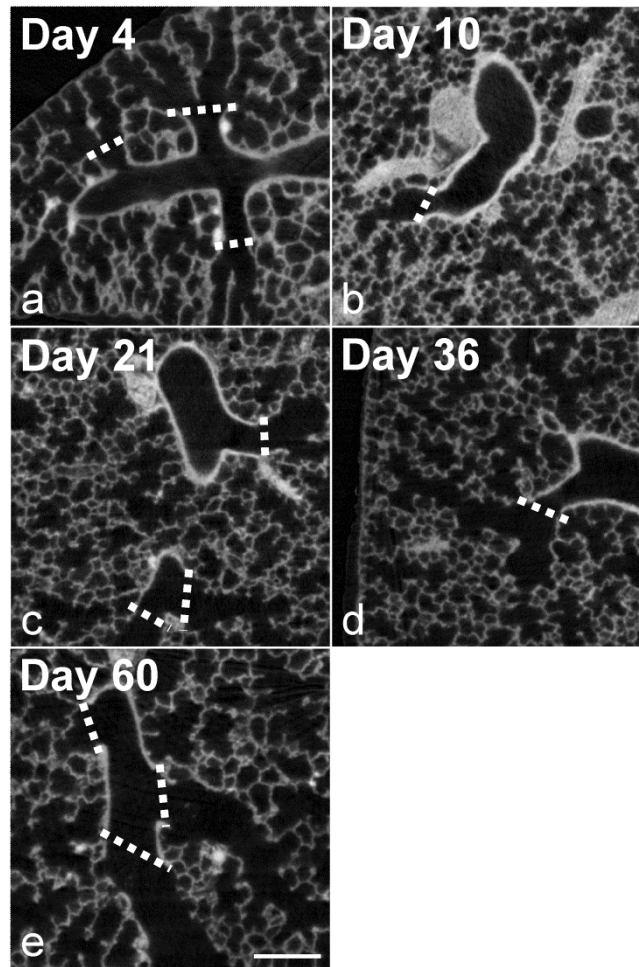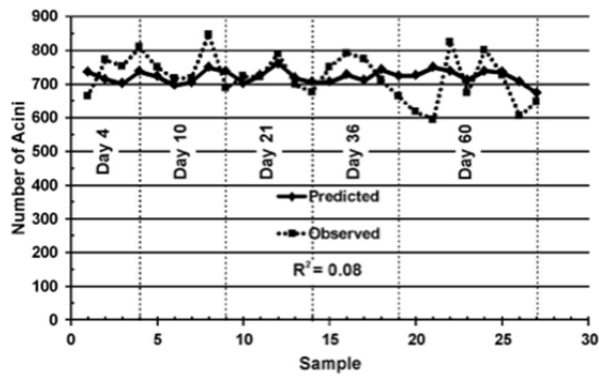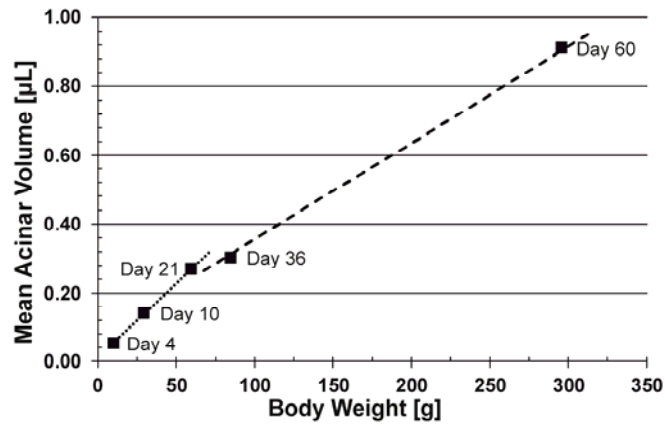
Figures

586

Figure 1. Acini, as they appear throughout lung development. At day 4 **(a)** only

588   sacculi and no alveoli are present. The walls of the conducting airways are smooth

and not much, but significantly thicker than the inter airspace wall of the parenchyma.

590   At day 10 (**b**) alveolarization evidently started; resulting in smaller parenchymal

airspace and a larger difference between the thickness of the walls of the conducting

592   and gas-exchanging airways. At the later days (21 – 60, **c-e**) the difference of the

wall thicknesses are becoming even more pronounced. Dotted lines mark acinar

594   entrances. Scale bar 250 µm.

596

Figure 2. Relationship between number of acini, lung volume, and body weight.

598   No linear correlation was observed between number of acini, body weight, and lung

volume. Thus, the number of acini cannot be estimated by these parameters.

600

Figure 3. Bi-phasic growth of the mean acinar airspace volume. The mean

602   acinar volume (tissue and airspace) grows in two distinct phases. Days 4-21:

proportional growth of acinar volume and body weight (R^2 = 0.954, dotted line). Days

604   36-60: no proportional growth (R^2 = 0.887, dashed line).
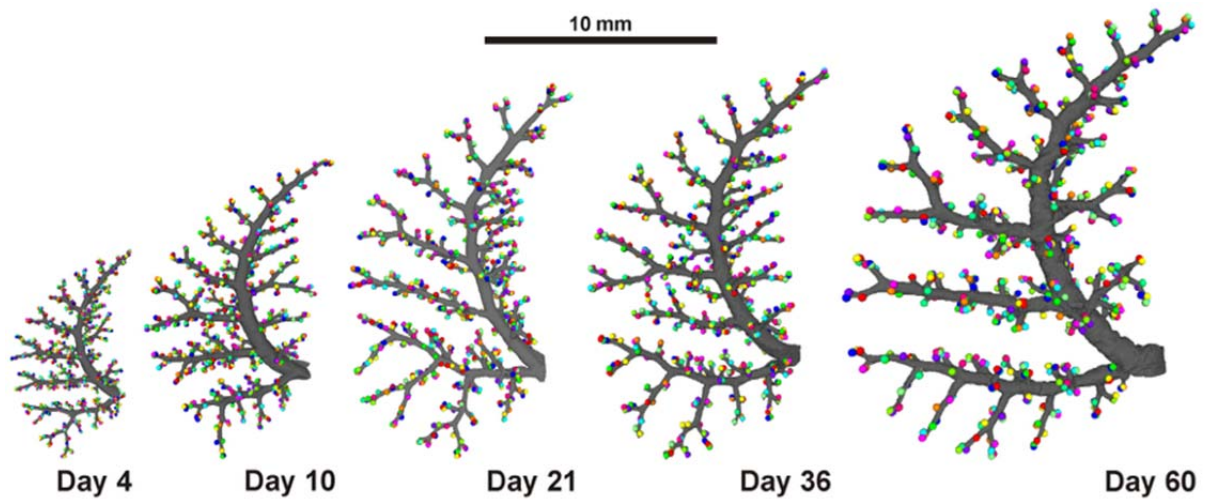
Figure 4. Trees of conducting airways throughout postnatal lung development. The walls of the conducting airways are shown in grey and the spheres represent the acini entrances. These three-dimensional visualizations show the large similarity of the conducting airways structure at days 4, 10, 21, 36, and 60 and between different individuals.

Tables

Volume density of parenchyma					
Postnatal day	**RUL**	**RML**	**RLL**	**LC**	**LL**
4	0.865	0.818	0.856	0.827	0.865
10		0.846			
21		0.869			
36		0.870			
60	0.888	0.839	0.843	0.865	0.862

612

Table 1. Volume density of the parenchyma. No significant differences were observed. RUL: right upper lobe; RML: right middle lobe; RLL: right lower lobe; LC: cardiac lobe; LL: left lung.

Postnatal Day	Fraction of Total Lung Volume [%]									
	RUL		RML		RLL		LC		LL	
	Mean	SD	Mean	SD	Mean	SD	Mean	SD	Mean	SD
4	11.15	0.81	12.37	0.88	29.68	2.50	5.86*	0.80	40.94*	2.35
10	11.75	1.27	13.08	1.49	30.72	2.89	11.87	1.59	32.59	5.80
21	11.04	0.75	12.68	0.51	29.69	0.72	10.69	0.28	35.90	0.99
36	10.74	0.70	12.37	0.60	30.40	0.54	10.87	0.66	35.62	0.92
60	10.89	0.83	12.49	1.14	28.49	1.17	12.69*	0.70	35.44	1.04
Mean of all days	11.09	0.89	12.59	0.97	29.66	1.80	-	-	-	-

616

Table 2. Fraction of the lung lobes of the total lung volume throughout lung development. Except of the cardiac lobe and the left lung the lobe volume increases in parallel to the growth of the total lung volume. At the cost of the left lung, the cardiac lobe increases disproportionately. RUL: right upper lobe; RML: right middle lobe; RLL: right lower lobe; LC: cardiac lobe; LL: left lung; SD: standard deviation; *: differs significantly (ANOVA) from the other time points for the same lobe.

	Mean acinar volume			Manual counting	
	Mean	STD	t-test	Mean	STD
	[µL]			[# Acini]	
RUL	0.065	0.014	0.556	766	70
RML	0.066	0.008		777	29
RLL	0.069	0.014	0.917	1841	175
LC	0.030	0.003	0.027 *	769	24
LL	0.105	0.017	0.001 *	1711	214
LC + LL	0.081	0.011	0.198	2481	210
Entire Lung	0.073	0.011	0.674	5865	465

624

Table 3. Comparison of the mean acinar volume and the number of acini per lobe at postnatal day 4. To validate the right middle lobe as an estimator for the entire lung, three entire lungs were manually counted. We observed that the right upper, middle, and low lobe, but not the cardiac lobe and the left lung represent a valid sample for the entire lung. RUL: right upper lobe; RML: right middle lobe; RLL: right lower lobe; LC: cardiac lobe, LL: left lung, SD: standard deviation, *: significantly differs (ANOVA) from the other time points for the same lobe.

Postnatal Day	Number of Samples	Body Weight [g]		Lung Volume [ml]		Number of Acini (RML) [# Acini]	
		Mean	SD	Mean	SD	Mean	SD
4	4	10.15	0.54	0.506	0.030	749[+]	62
10	5	29.42	3.22	1.32	0.102	743[+]	61
21	5	59.65	2.05	2.32	0.136	721[+]	42
36	5	84.75	9.65	2.80	0.271	738[+]	52
60	8	295.82	16.77	7.51	0.544	686[+]	89
Mean of all days	27					722	67

632

Table 4. Comparison of the body weight, lung volume and number of acini.

634   RML: right middle lobe, SD: standard deviation, [+]: no significant difference.

Postnatal Day	Mean Acinar Volume [µl]		Specific Mean Acinar Volume [µl / 100 g]	
	Mean	SD	Mean	SD
4	0.069*	0.007	0.678	0.075
10	0.196*	0.017	0.677	0.115
21	0.355+	0.027	0.596	0.055
36	0.410+	0.050	0.484*	0.019
60	1.157*	0.138	0.393*	0.064

636 **Table 5 Mean acinar volume**. Parenchymal lobe volume divided by the counted number of acini, Specific mean acinar volume: mean acinar volume per 100 g body 638 weight, *: differs significantly (ANOVA) from the other time points, +: the mean acinar volume of days 21 and 36 are not significantly different from each other, however 640 they are both significantly different form the three other time points.